PHYSICAL REVIEW B **94**, 220301(R) (2016)

Phonon anharmonicity, lifetimes, and thermal transport in $CH_3NH_3PbI_3$ from many-body perturbation theory

Lucy D. Whalley,[1] Jonathan M. Skelton,[2] Jarvist M. Frost,[1,2] and Aron Walsh[1,2,3,*]

[1]*Department of Materials, Imperial College London, Exhibition Road, London SW7 2AZ, United Kingdom*

[2]*Department of Chemistry, University of Bath, Claverton Down, Bath BA2 7AY, United Kingdom*

[3]*Global E[3] Institute and Department of Materials Science and Engineering, Yonsei University, Seoul 120-749, Korea*

(Received 30 August 2016; revised manuscript received 12 October 2016; published 8 December 2016)

Lattice vibrations in $CH_3NH_3PbI_3$ are strongly interacting, with double-well instabilities present at the Brillouin zone boundary. Analysis within a first-principles lattice-dynamics framework reveals anharmonic potentials with short phonon quasiparticle lifetimes and mean free paths. The phonon behavior is distinct from the inorganic semiconductors GaAs and CdTe where three-phonon interaction strengths are three orders of magnitude smaller. The implications for the applications of hybrid halide perovskites arising from thermal conductivity, band-gap deformation, and charge-carrier scattering through electron-phonon coupling, are presented.

DOI: 10.1103/PhysRevB.94.220301

Hybrid halide perovskites have been the subject of intensive investigation due to their strong photovoltaic action [1]. While solar-cell device efficiencies are high, our understanding of the materials properties remains limited in comparison. Here we address the anharmonic nature of phonons in $CH_3NH_3PbI_3$ from a theoretical perspective, with a particular focus on phonon interactions, lifetimes, and coupling to the electronic structure.

Lattice vibrations of hybrid perovskites. Vibrational spectroscopy is a valuable tool in materials characterization. As such, there have been multiple reports concerning the IR and Raman activity of $CH_3NH_3PbI_3$ [2–7]. Chemical breakdown to PbI_2 is a concern, but once careful measurements are made, satisfactory agreement can be obtained between first-principles theory and experiment [5,7]. As expected from the large difference in atomic mass, vibrations of the PbI_3^- framework are found at lower energy (0–5 THz) with $CH_3NH_3^+$ vibrations at higher energy (8–100 THz); however, significant coupling is found between the two, as explored in our earlier work [7] and observed in neutron scattering measurements on $CH_3NH_3PbBr_3$ [8].

Harmonic phonon dispersion. The potential energy (U) of a crystal can be expanded as a Taylor series of ionic displacements (r). The static crystal potential (U_0) has no bearing on the dynamics, and for a relaxed structure the $\frac{dU}{dr}$ term is zero. In the harmonic approximation only the $\frac{d^2U}{dr^2}$ term is considered. The phonon eigenmodes from the solution of the dynamical matrix are orthogonal (and therefore noninteracting). While a number of salient features of the thermal physics can be reproduced by harmonic lattice dynamics, the resulting phonon modes have temperature-independent frequencies and possess infinite lifetimes. The quasiharmonic approximation (QHA), where harmonic potentials are calculated over a specified volume range, was developed to deal with the first issue, while phonon-phonon interactions must be considered for an explicit treatment of the second issue.

The harmonic phonon dispersion for $CH_3NH_3PbI_3$ in the low-temperature orthorhombic and high-temperature cubic phases is shown in Fig. 1. We use the same computational setup previously reported [7] based on PHONOPY [9], VASP [10], and the PBEsol exchange-correlation functional [11] (see Supplemental Material [12]). There is significant dispersion across the vibrational Brillouin zone in the low-frequency modes. We focus on the region up to 5 THz where vibrations of the PbI_3^- framework are found. While IR and Raman spectroscopy probe the Γ-point ($q = 0$) modes, this represents a small fraction of the possible lattice vibrations. All of the phonon modes in the orthorhombic phase have zero or positive frequencies. Two imaginary frequency acoustic modes are found in the cubic phase, centered around the R ($q = \frac{1}{2},\frac{1}{2},\frac{1}{2}$) and M ($q = \frac{1}{2},\frac{1}{2},0$) special points. These indicate the presence of a saddle point in the potential-energy surface, and thus that the structure is not dynamically stable. Such "soft" or "imaginary" modes have been recently observed in inelastic x-ray scattering measurements of the phonon dispersion [13,14].

Soft phonon modes. The imaginary acoustic phonon modes at R and M are zone-boundary instabilities characteristic of the perovskite crystal structure [15,16]. They are associated with collective tilting of the corner-sharing octahedral framework, as observed in molecular dynamics [17,18]. The same instabilities have been reported in $CsSnI_3$ [19,20], where they persist even in QHA calculations [21]. These zone-boundary motions can be described within a computationally tractable $2 \times 2 \times 2$ supercell expansion of the cubic perovskite lattice. Within the frozen-phonon approximation, we map out the potential-energy surface for displacement along the imaginary zone-boundary eigenvectors (Fig. 2). By following the imaginary-mode eigenvectors to map the potential-energy surface, we are assuming that both the mode eigenvector and potential-energy surface are set by the crystal symmetry. The result is a characteristic double-well potential, where the cubic perovskite structure is a saddle point between two equivalent broken-symmetry solutions. The barriers are significant (37 and 19 meV for the R and M modes, respectively) and are comparable to k_BT, so order-disorder behavior is expected [22].

The phase transitions from cubic to tetragonal and orthorhombic perovskite structures can be understood as a condensation of the R and subsequently M modes [16]. Similar transitions are observed in $CsPbCl_3$ [23]. To further understand the physical behavior we have solved the time-independent

*a.walsh@imperial.ac.uk

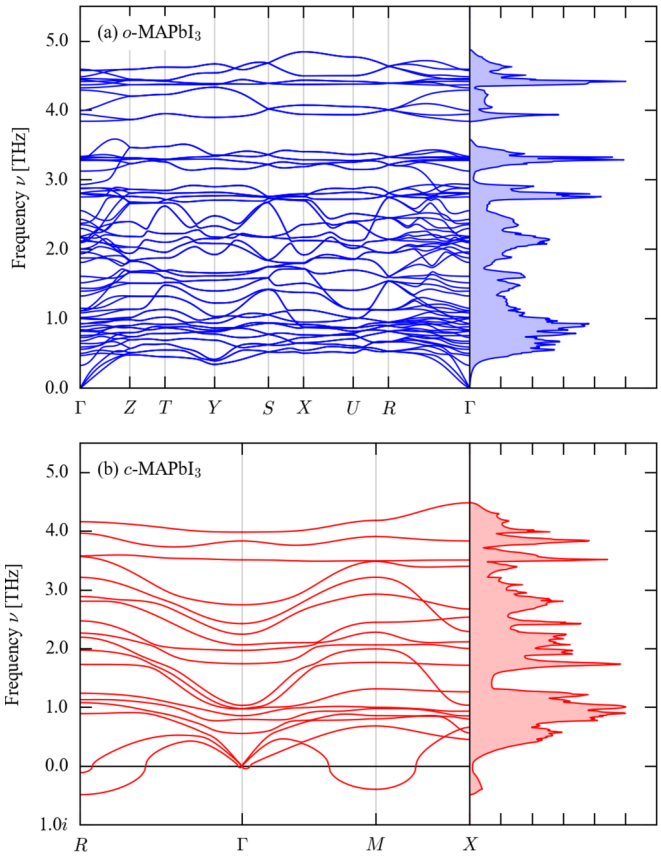

FIG. 1. Harmonic phonon dispersion up to 5 THz in the (a) low-temperature (orthorhombic) and (b) high-temperature (cubic) perovskite phases of $CH_3NH_3PbI_3$. They are calculated from lattice dynamics using forces from density-functional theory (PBEsol electron exchange and correlation).

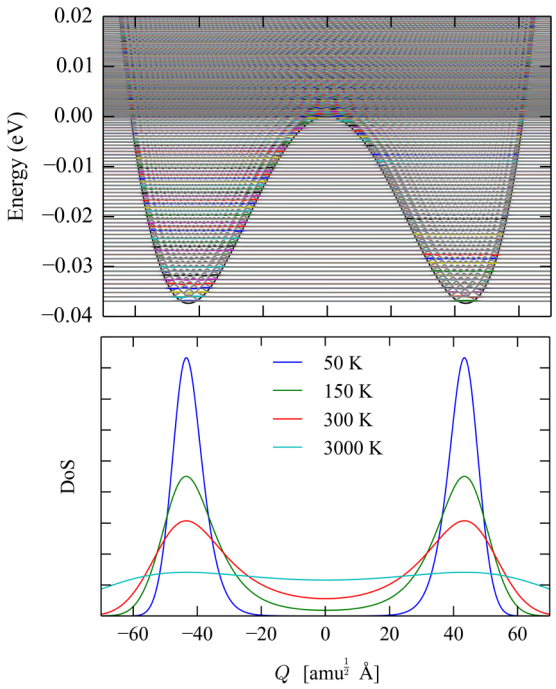

FIG. 2. Potential-energy surface from frozen-phonon calculations of the imaginary eigenmode present at the R point in the high-temperature perovskite phase of $CH_3NH_3PbI_3$. Q represents the normal mode coordinate (phonon amplitude). The solution of a 1D Schrödinger equation (states shown as horizontal lines with wave functions in the upper panel) are used to generate a thermalized probability density of states (DOS; lower panel).

Schrödinger equation describing the nuclear motion in this one-dimensional (1D) double-well potential. The procedure, outlined in Ref. [24], makes a single-phonon approximation and neglects coupling to other phonon modes. It assumes that energetic cross terms from interaction with the other modes are small, which is expected for such rigid octahedral tilts. A similar scheme, based on a similar independent-mode approximation, has recently been reported by Adams and Passerone [25].

The resulting eigenstates form a partition function which can be associated with a renormalized harmonic frequency that reproduces the thermodynamic contribution of the anharmonic system [24]. Values of 0.08 THz (M) and 0.10 THz (R) are found for $T = 300$ K. Since the phonon occupation is governed by Bose-Einstein statistics, these low-energy modes are highly populated, as has been evidenced in x-ray scattering experiments [13,14].

Phonon lifetimes and mean free paths. We next consider three-phonon interactions via a peturbative many-body expansion as implemented in PHONO3PY [9,26,27]. To provide a reference point, we have performed equivalent calculations on the inorganic semiconductors GaAs and CdTe (both zinc-blende-type structures), with the results compared in Fig. 3. The difference in behavior is striking with the average strength of three-phonon interactions three orders of magnitude larger in $CH_3NH_3PbI_3$, which results in lifetimes (τ) three orders of magnitude *shorter* in the hybrid perovskite. While phonon mean free paths of up to 10 μm are found in CdTe and GaAs, for $CH_3NH_3PbI_3$ the limit is 10 nm.

Thermal conductivity. Lattice thermal conductivity can be expressed as the tensor product of the modal heat capacity (C_V), group velocity ($\mathbf{v}$), and phonon mean free path ($\Lambda = \mathbf{v}\tau$) summed over all modes (λ) and averaged over wave vectors (q). The result, based upon the values determined from the anharmonic lattice-dynamics calculations, is that $CH_3NH_3PbI_3$ is a thermal insulator in comparison to GaAs and CdTe. The combination of short mode lifetimes and low group velocities (Fig. 3) results in a low averaged thermal conductivity of $0.05\,\mathrm{W\,m^{-1}\,K^{-1}}$ at $T = 300$ K (Fig. 4). The "ultralow" thermal conductivity is in agreement with previous calculations and experiments that highlighted potential applications for heat-to-electricity conversion in thermoelectric devices [28–30].

Low-lying acoustic modes are responsible for conducting the majority of the heat in CdTe and GaAs. Due to the unusually short lifetimes of these modes in $CH_3NH_3PbI_3$, it is the cage modes in the 1–3 THz window that make the dominant contribution. While the molecular vibrations (up to 100 THz) influence the lifetimes and mean free paths of the low-frequency inorganic cage modes, they do not directly contribute to thermal transport.

Carrier scattering. The scattering of charge carriers (electrons and holes) in semiconductors is determined by the sum of the rates of all possible processes. It is common to identify the

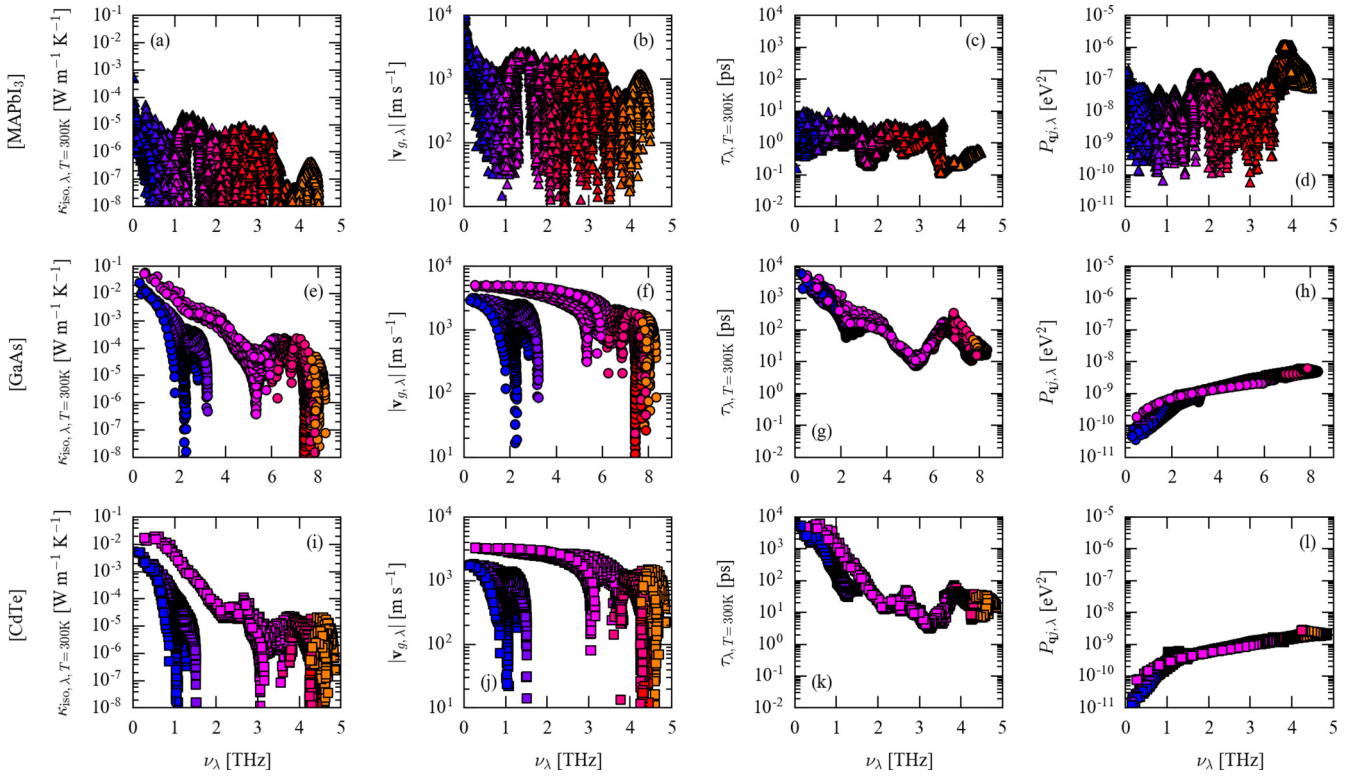

FIG. 3. Results from anharmonic lattice-dynamics calculations on $CH_3NH_3PbI_3$, GaAs, and CdTe. Average phonon modal interaction strength (P) and group velocity ($\mathbf{v}$), as well as the $T = 300$ K values of modal lifetime (τ) and thermal conductivity (κ) are shown. Only the 0–5 THz range is shown for $CH_3NH_3PbI_3$. The data points are colored according to the band index.

dominant scattering mechanism in a sample by the temperature dependence of the transport properties. While simple textbook relationships exist, they are usually for idealized systems, e.g., for harmonic vibrations and parabolic electronic bands. Hybrid perovskites are nonstandard semiconductors: they are mechanically soft, the vibrations are anharmonic, the bands

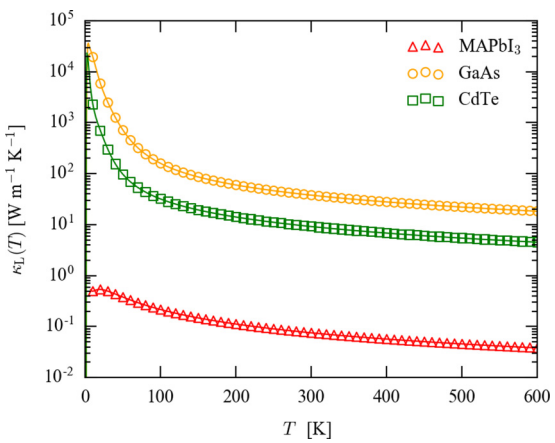

FIG. 4. Lattice thermal conductivity of $CH_3NH_3PbI_3$, GaAs, and CdTe calculated from three-phonon interactions within the relaxation time approximation (excluding isotope effects). The calculated values of 38 W m^{-1} K^{-1} (GaAs) and 9 W m^{-1} K^{-1} (CdTe) at $T = 300$ K compare well to the measured values of 45 and 7 W m^{-1} K^{-1}, respectively [31]. The corresponding value calculated for $CH_3NH_3PbI_3$ is 0.05 W m^{-1} K^{-1} .

are nonparabolic [32], and the dielectric constants are strongly temperature dependent [33]. Deviations from basic models should be expected.

Analysis of photoconductivity data pointed towards dominant acoustic deformation potential scattering in hybrid perovskites due to a $T^{-\frac{3}{2}}$ dependence of the scattering time for $150 < T < 300$ K [34]. Similar results have been reported from Hall measurements [35]. As the lattice volume fluctuates in thermal equilibrium, so do the valence- and conduction-band energies [36]. In support of this model, the band-gap deformation potential has been calculated to be large [37] and the elastic constants are small [38]. However, for heteropolar materials optical phonon scattering is usually the dominant mechanism at high temperatures [39]. As hybrid perovskites possess low-frequency optical phonons, the crossover temperature is likely to be below 300 K [40]. Recent analysis of emission line broadening highlighted the role of longitudinal optical phonons (the Fröhlich interaction), where the photoluminescence linewidth at $T = 300$ K was broken down into inhomogeneous broadening (26 meV) and optic-mode broadening (40 meV) components [41]. Numerical simulations of scattering kinetics clearly show that the $T^{-\frac{3}{2}}$ behavior can be explained by optic-mode events [42].

Anharmonic band-gap deformation. A common method used to calculate electron-phonon coupling is density-functional perturbation theory (DFPT) [43]. DFPT assumes and requires a small harmonic response for the perturbative treatment to be correct. For anharmonic phonon modes, where the range of motion is large, these assumptions do not hold.

Previous studies on hybrid perovskites have only considered (positive-frequency) harmonic phonons [41,44].

We return to earlier theories of electron-phonon interaction based on the phonon-frozen approximation and adiabatic decoupling of the nuclear and electronic degrees of freedom [45,46]. To estimate the effect of the anharmonic potential-energy surface on the electronic structure of $CH_3NH_3PbI_3$, we calculated the change in band gap $\Delta E_g(Q)$ with respect to the imaginary-mode phonon amplitude. A similar band-gap deformation is found for the M and R modes. The effect of tilt angle on band gap has been explored in other studies [47,48], however, the present analysis quantifies it for a collective phonon mode. We find that $E_g(Q)$ is well described as quadratic over small Q, but required a biquadratic term to reproduce the correct behavior at large Q.

The expectation value of E_g as a function of temperature (T) can be written as

$$E_g(T) = \langle \chi(Q,T)|E_g(Q)|\chi(Q,T)\rangle, \quad (1)$$

where χ is the thermally populated vibrational wave function obtained from solving the 1D Schrödinger equation (Fig. 2). All calculations are reduced to the collective phonon coordinate Q, making them computationally tractable. This, naturally, means that all cross terms are discounted.

Summing $\Delta E_g(Q)$ multiplied by the vibrational probability density along Q yields a thermally averaged electron-phonon coupling for each mode. A biquadratic fit to the deformation potential was found to be essential, due to the considerable contribution from the large Q component of the wave function; using a harmonic approximation for $\Delta E_g(Q)$ led to solutions twice as large. This procedure does not assume that the wave function is centered around $Q = 0$. We estimate a positive band-gap shift of 35.5 meV (R mode) and 27.9 meV (M mode) at $T = 300$ K, which is comparable in magnitude to the measured broadening of 40 meV [41]. The anharmonic electron-phonon coupling of the soft modes in halide perovskites is therefore considerable, which merits further investigation.

In summary, we have explored the anharmonic nature of the phonons in $CH_3NH_3PbI_3$ and their effect on the physical properties of the material. We have predicted the existence of double-well potentials associated with octahedral tilting, provided insights into the strength of the phonon-phonon interactions and thermal transport, and highlighted the role of anharmonicity in electron-phonon interactions. We did not discuss the rotational activity of $CH_3NH_3^+$, which has been the subject of thorough investigation [4,8,49,50], and can be considered as an additional anharmonic perturbation. Neither have we discussed ion migration, which is a process that can also contribute to thermal properties including nonequilibrium thermoelectric power [51]. In conventional photovoltaic materials such as GaAs both the electronic and phonon mean free paths can exceed 1 μm [39], while for $CH_3NH_3PbI_3$ the path (limited to 10 nm) is much shorter, which may have important implications for hot-carrier cooling and nonradiative recombination processes during solar-cell operation.

Acknowledgments. We thank F. Brivio for preliminary phonon computations, and J. Buckeridge for assistance with the soft-mode analysis. This work was funded by the EPSRC (Grants No. EP/M009580/1, No. EP/K016288/1, No. EP/L01551X/1, and No. EP/K004956/1), the Royal Society, and the ERC (Grant No. 277757). Calculations were performed on the UK Archer HPC facility, accessed through membership of the UK HPC Materials Chemistry Consortium (EPSRC Grant No. EP/L000202) and the SiSu supercomputer at the IT Center for Science (CSC), Finland, via the Partnership for Advanced Computing in Europe (PRACE) Project No. 13DECI0317/IsoSwitch. We also made use of the Balena HPC facility at the University of Bath, which is maintained by Bath University Computing Services.

Data access statement. The crystal structures and phonon data are available at https://github.com/WMD-group/Phonons and https://doi.org/10.15125/BATH-00322. Codes to estimate anharmonic electron-phonon coupling are available from https://github.com/jarvist/Julia-SoftModeTISH-DeformationPotential.

[1] S. D. Stranks and H. J. Snaith, Nat. Nanotechnol. **10**, 391 (2015).

[2] C. Quarti, G. Grancini, E. Mosconi, P. Bruno, J. M. Ball, M. M. Lee, H. J. Snaith, A. Petrozza, and F. De Angelis, J. Phys. Chem. Lett. **5**, 279 (2014).

[3] M. Ledinský, P. Löper, B. Niesen, J. Holovský, S.-J. Moon, J.-H. Yum, S. De Wolf, A. Fejfar, and C. Ballif, J. Phys. Chem. Lett. **6**, 401 (2015).

[4] A. A. Bakulin, O. Selig, H. J. Bakker, Y. L. A. Rezus, C. Müller, T. Glaser, R. Lovrincic, Z. Sun, Z. Chen, A. Walsh, J. M. Frost, and T. L. C. Jansen, J. Phys. Chem. Lett. **6**, 3663 (2015).

[5] M. A. Pérez-Osorio, R. L. Milot, M. R. Filip, J. B. Patel, L. M. Herz, M. B. Johnston, and F. Giustino, J. Phys. Chem. C **119**, 25703 (2015).

[6] T. Glaser, C. Müller, M. Sendner, C. Krekeler, O. E. Semonin, T. D. Hull, O. Yaffe, J. S. Owen, W. Kowalsky, A. Pucci, and R. Lovrinčić, J. Phys. Chem. Lett. **6**, 2913 (2015).

[7] F. Brivio, J. M. Frost, J. M. Skelton, A. J. Jackson, O. J. Weber, M. T. Weller, A. R. Goni, A. M. A. Leguy, P. R. F. Barnes, and A. Walsh, Phys. Rev. B **92**, 144308 (2015).

[8] I. P. Swainson, C. Stock, S. F. Parker, L. Van Eijck, M. Russina, and J. W. Taylor, Phys. Rev. B **92**, 100303 (2015).

[9] A. Togo and I. Tanaka, Scr. Mater. **108**, 1 (2015).

[10] G. Kresse and J. Furthmüller, Phys. Rev. B **54**, 11169 (1996).

[11] J. P. Perdew, A. Ruzsinszky, G. I. Csonka, O. A. Vydrov, G. E. Scuseria, L. A. Constantin, X. Zhou, and K. Burke, Phys. Rev. Lett. **100**, 136406 (2008).

[12] See Supplemental Material at http://link.aps.org/supplemental/10.1103/PhysRevB.94.220301 for the technical setup and more detailed plots concerning phonon anharmonicity and thermal conductivity.

[13] A. N. Beecher, O. E. Semonin, J. M. Skelton, J. M. Frost, W. Maxwell, H. Zhai, A. Alatas, J. S. Owen, A. Walsh, and S. J. L. Billinge, ACS Energy Lett. **1**, 880 (2016).

[14] R. Comin, M. K. Crawford, A. H. Said, N. Herron, W. E. Guise, X. Wang, P. S. Whitfield, A. Jain, X. Gong, A. J. H. McGaughey, and E. H. Sargent, Phys. Rev. B **94**, 094301 (2016).
[15] P. M. Woodward, Acta Crystallogr., Sect. B: Struct. Sci. **53**, 32 (1997).
[16] H. T. Stokes, E. H. Kisi, D. M. Hatch, and C. J. Howard, Acta Cryst. B **58**, 934 (2002).
[17] J. M. Frost, K. T. Butler, and A. Walsh, APL Mater. **2**, 081506 (2014).
[18] C. Quarti, E. Mosconi, J. M. Ball, V. D'Innocenzo, C. Tao, S. Pathak, H. J. Snaith, A. Petrozza, and F. De Angelis, Energy Environ. Sci. **16**, 155 (2016).
[19] L. Y. Huang and W. R. L. Lambrecht, Phys. Rev. B **90**, 195201 (2014).
[20] C. E. Patrick, K. W. Jacobsen, and K. S. Thygesen, Phys. Rev. B **92**, 201205 (2015).
[21] E. L. da Silva, J. M. Skelton, S. C. Parker, and A. Walsh, Phys. Rev. B **91**, 144107 (2015).
[22] M. Dove, Am. Mineral. **82**, 213 (1997).
[23] Y. Fujii, S. Hoshino, Y. Yamada, and G. Shirane, Phys. Rev. B **9**, 4549 (1974).
[24] J. M. Skelton, L. A. Burton, S. C. Parker, A. Walsh, C.-E. Kim, A. Soon, J. Buckeridge, A. A. Sokol, C. R. A. Catlow, A. Togo, and I. Tanaka, Phys. Rev. Lett. **117**, 075502 (2016).
[25] D. J. Adams and D. Passerone, J. Phys.: Condens. Matter **28**, 305401 (2016).
[26] A. Togo, L. Chaput, and I. Tanaka, Phys. Rev. B **91**, 094306 (2015).
[27] J. M. Skelton, S. C. Parker, A. Togo, I. Tanaka, and A. Walsh, Phys. Rev. B **89**, 205203 (2014).
[28] A. Pisoni, J. Jaćimović, O. S. Barišić, M. Spina, R. Gaál, L. Forró, and E. Horváth, J. Phys. Chem. Lett. **5**, 2488 (2014).
[29] Y. He and G. Galli, Chem. Mater. **26**, 5394 (2014).
[30] X. Mettan, R. Pisoni, P. Matus, A. Pisoni, J. Jacimovic, B. Náfrádi, M. Spina, D. Pavuna, L. Forró, and E. Horváth, J. Phys. Chem. C **119**, 11506 (2015).
[31] O. M. Madelung, *Semiconductors: Data Handbook*, 3rd ed. (Springer, Berlin, 2003), p. 691.
[32] F. Brivio, K. T. Butler, A. Walsh, and M. van Schilfgaarde, Phys. Rev. B **89**, 155204 (2014).
[33] N. Onoda-Yamamuro, T. Matsuo, and H. Suga, J. Phys. Chem. Solids **53**, 935 (1992).
[34] M. Karakus, S. A. Jensen, F. D'Angelo, D. Turchinovich, M. Bonn, and E. Canovas, J. Phys. Chem. Lett. **6**, 4991 (2015).
[35] H. T. Yi, X. Wu, X. Zhu, and V. Podzorov, Adv. Mater. **28**, 6509 (2016).
[36] J. Bardeen and W. Shockley, Phys. Rev. **80**, 72 (1950).
[37] J. M. Frost, K. T. Butler, F. Brivio, C. H. Hendon, M. van Schilfgaarde, and A. Walsh, Nano Lett. **14**, 2584 (2014).
[38] S. Sun, Y. Fang, G. Kieslich, T. White, and T. Cheetham, J. Mater. Chem. A **3**, 18450 (2015).
[39] M. Cardona and N. E. Christensen, Phys. Rev. B **35**, 6182 (1987).
[40] A. M. A. Leguy, A. R. Goñi, J. M. Frost, J. Skelton, F. Brivio, X. Rodríguez-Martínez, O. J. Weber, A. Pallipurath, M. I. Alonso, M. Campoy-Quiles, M. T. Weller, J. Nelson, A. Walsh, and P. R. F. Barnes, Phys. Chem. Chem. Phys. **18**, 27051 (2016).
[41] A. D. Wright, C. Verdi, R. L. Milot, G. E. Eperon, M. A. Pérez-Osorio, H. J. Snaith, F. Giustino, M. B. Johnston, and L. M. Herz, Nat. Commun. **7**, 11755 (2016).
[42] A. Filippetti, A. Mattoni, C. Caddeo, M. I. Saba, and P. Delugas, Phys. Chem. Chem. Phys. **18**, 15352 (2016).
[43] S. Baroni and S. D. Gironcoli, Rev. Mod. Phys. **73**, 515 (2001).
[44] H. Kawai, G. Giorgi, A. Marini, and K. Yamashita, Nano Lett. **15**, 3103 (2015).
[45] L. J. Sham and J. M. Ziman, Solid State Phys. **15**, 221 (1963).
[46] B. Monserrat, N. D. Drummond, and R. J. Needs, Phys. Rev. B **87**, 144302 (2013).
[47] M. R. Filip, G. E. Eperon, H. J. Snaith, and F. Giustino, Nat. Commun. **5**, 5757 (2014).
[48] A. Amat, E. Mosconi, E. Ronca, C. Quarti, P. Umari, M. K. Nazeeruddin, M. Grätzel, and F. De Angelis, Nano Lett. **14**, 3608 (2014).
[49] A. M. A. Leguy, J. M. Frost, A. P. McMahon, V. G. Sakai, W. Kochelmann, C. Law, X. Li, F. Foglia, A. Walsh, B. C. O'Regan, J. Nelson, J. T. Cabral, and P. R. F. Barnes, Nat. Commun. **6**, 7124 (2015).
[50] T. Chen, B. J. Foley, B. Ipek, M. Tyagi, J. R. D. Copley, C. M. Brown, J. J. Choi, and S.-H. Lee, Phys. Chem. Chem. Phys. **17**, 31278 (2015).
[51] A. R. Allnatt and P. W. M. Jacobs, Proc. R. Soc. London, Ser. A **260**, 350 (1961).